A Novel Balanced Nonreciprocal Bandpass Filter Based on Stepped-Impedance Resonator and Time-Modulated Resonator

Peng HAN [1], Zhongbao WANG [1, 2], Hongmei LIU [1], Mingming GAO [2], Shaojun FANG [1]

[1] School of Information Science and Technology, Dalian Maritime University, Dalian, Liaoning 116026, China
[2] Liaoning Key Laboratory of Radio Frequency and Big Data for Intelligent Applications, Liaoning Technical University, Huludao, Liaoning 125105, China

hanpeng2022@dlmu.edu.cn, wangzb@dlmu.edu.cn

Submitted June 6, 2024 / Accepted August 7, 2024 / Online first August 16, 2024

Abstract. *A novel balanced nonreciprocal bandpass filter based on the stepped impedance resonator and the time-modulated resonator is proposed in this paper. The balanced nonreciprocal bandpass filter is fabricated on a single PCB board, and the compact structure is achieved through the gap coupling structure of the microstrip resonators. Utilizing the quarter-wavelength transformer and gap coupling structure, good isolation between RF and modulated signals is achieved without adding lumped elements. Relying on the efficient modulation circuit and the half-wavelength stepped impedance resonator's inherent resonance characteristic, an excellent nonreciprocal characteristic of the differential signal and effective suppression of common-mode noise are achieved. A balanced microstrip nonreciprocal bandpass filter operating at the center frequency of 1.5 GHz is designed, simulated, and experimentally verified. The measured reverse isolation is greater than 20 dB with a bandwidth of 48.8 MHz. The measured forward differential-mode insertion loss is 3.7 dB at the center frequency of 1.5 GHz. In the range of 1.2–1.8 GHz, the measured common-mode noise suppression is larger than 60.4 dB.*

Keywords

Balanced bandpass filters, nonreciprocal filter, stepped-impedance resonators, time-modulated resonators, common-mode noise suppression

1. Introduction

The demand for network capacity has significantly increased due to the rapid progress of wireless communication networks. The utilization of spectrum can be practically doubled by the implementation of full-duplex technology, making it an important solution [1], [2]. One essential characteristic of a full-duplex system is its unidirectional characteristic, where nonreciprocal devices are critical for simultaneous delivery and receipt of information. Ferrite has been utilized in nonreciprocal devices for a long period of time. However, ferrite-based nonreciprocal devices have drawbacks, such as their large size and difficult integration [3], [4]. Most of the magnetless nonreciprocal devices that have been developed and employed are based on transistor-based configurations [5], [6]. However, the noise that the active devices produce restricts this type of nonreciprocal device [7]. Nonreciprocal devices based on time-modulated resonators (TMRs) can address these drawbacks.

Noise degrades the performance of wireless communication systems, and efficient use of spectrum resources necessitates the circuit's anti-jamming capability. The balanced filter can suppress common-mode noise, reduce electromagnetic interference, and thus improve the efficient utilization of specific spectrum resources [8], [9]. Reconfigurable, reflectionless, and other multi-functional balanced filters have received widespread attention [10], [11].

For the first time, Wu et al. proposed a nonreciprocal filter with TMRs using lumped elements [12]. Subsequently, nonreciprocal filters using TMRs have been extensively studied [13–15]. Simultaneously, its matrix numerical analysis has gone through investigation [16], [17]. The balanced nonreciprocal bandpass filter based on the TMR has the characteristics of low noise, easy integration, and strong anti-interference ability. However, research on balanced nonreciprocal bandpass filters is still limited. Only one balanced nonreciprocal filter has been reported [18], but its issues of large size, complex structure, and narrow reverse isolation bandwidth need to be addressed.

In this paper, a novel balanced nonreciprocal bandpass filter (BPF) based on the stepped impedance resonator (SIR) and the time-modulated resonator is presented for the first time. The differential-mode (DM) bandpass filtering and common-mode (CM) noise suppression are realized through the gap coupling structure of the resonators and the inherent resonance characteristic of the SIR (each resonant frequency corresponds to a symmetric or an anti-symmetric voltage distribution on the resonator). At the same

DOI: 10.13164/re.2024.0487

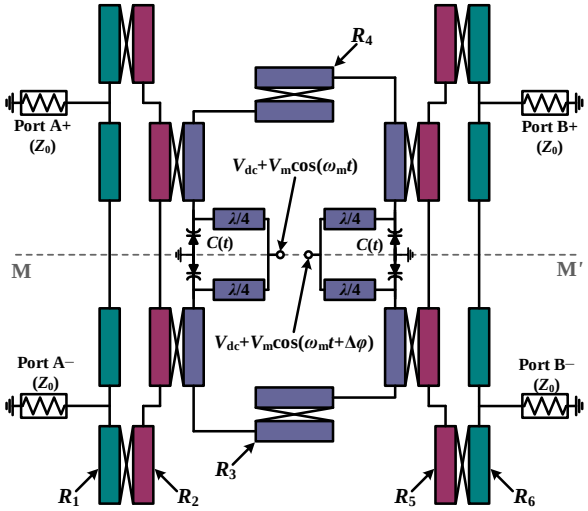

Fig. 1. Schematic of the proposed balanced nonreciprocal BPF.

time, utilizing the quarter-wavelength transformer, a simple and compact isolation structure between RF and modulated signals is realized. Meanwhile, two poles generated by two TMRs yield an improved nonreciprocal performance in reverse isolation. The subsequent sections present an analysis of the circuit structure, parameterization of the modulation parameters, and verification of the theory through a practical measurement.

2. Filter Structure and Theoretical Analysis

Figure 1 shows the circuit schematic of the proposed balanced nonreciprocal BPF, which is constructed by four SIRs and two TMRs, which are equivalent to a half-wavelength resonator at the center frequency f_0. Specifically, R_i (i = 1, 2, 5, 6) are SIRs, in which R_1 and R_6 load the balanced RF input ports A (including ports A+ and A−) and the balanced RF output port B (including ports B+ and B−) through tapped coupling, respectively. The resonators R_3 and R_4 are TMRs. In order to achieve nonreciprocal characteristics, four reverse biased varactor diodes are loaded symmetrically at the midpoint of the resonators R_3 and R_4, which load the bias voltage and the modulation signal via the $\lambda/4$ microstrip lines.

The TMR is modulated with reverse biased varactor diodes as follows:

$$C(t) = C_0 + \Delta C \cos(\omega_m t + \Delta\varphi) \tag{1}$$

where C_0 is the nominal (DC) capacitance, ΔC is the modulation depth corresponding to the modulation voltage V_m, $f_m = \omega_m/(2\pi)$ is the modulation frequency, and $\Delta\varphi$ is the progressive phase shift of the modulating signal [12].

At the center frequency f_0, the time-modulated resonator's resonance characteristic remains unaffected by the $\lambda/4$ microstrip line, which can be considered to be an open-circuit. Meanwhile, all resonators possess an identical fundamental resonant frequency f_0, and the filter structure is symmetrical corresponding to the plane MM′, as shown in Fig. 1.

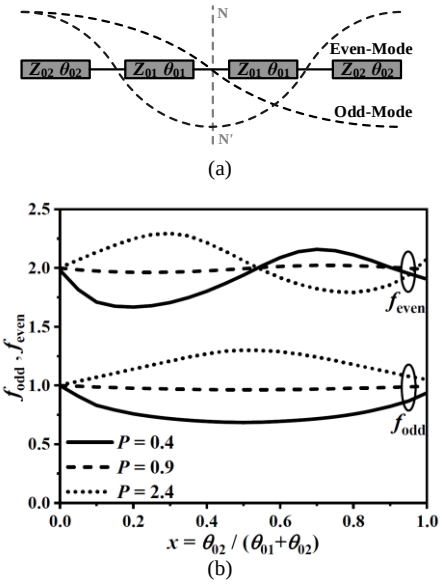

Fig. 2. (a) Structure of SIR and (b) normalized resonant frequencies of SIR.

2.1 Resonator Analysis

Figure 2(a) gives the structure of a typical SIR, which has a mirror structure corresponding to the plane NN′. Therefore, the SIR can be further analyzed by even- and odd-mode method. At this point, the vertical symmetry plane of the SIR serves as an electric wall or a magnetic wall according to the boundary conditions of the symmetric plane [19]. The resonance condition can be derived as:

$$\begin{cases} \cot\theta_{01} = -P\cot\theta_{02} & \text{(odd-mode)} \\ \tan\theta_{01} = P\cot\theta_{02} & \text{(even-mode)} \end{cases} \tag{2}$$

where $P = Z_{02}/Z_{01}$ is the impedance ratio of the SIR. The SIR has an infinite number of resonant frequencies. The fundamental resonance occurs in the odd-mode and the first higher-order resonance in the even-mode. In order to clarify the relationship between the resonant frequencies of interest in the balanced circuit and the impedance ratio P, the normalized odd-mode resonant frequencies and even-mode resonant frequencies against $x = \theta_{02}/(\theta_{01}+\theta_{02})$ are plotted in Fig. 2(b) for Z_{01} = 50 Ohm and P = 0.4, 0.9, and 2.4. From the resonant frequency curve of Fig. 2(b), it can be observed that the physical dimensions of the SIR can be adjusted by controlling the impedance ratio, which helps to achieve a reasonable BPF layout. Meanwhile, it can be observed that the first higher order resonance occurs in the even-mode, which means the common-mode signal will not be excited at the center frequency f_0.

As shown in Fig. 3(a), the TMRs R_3 and R_4 are initially $\lambda_g/2$ uniform impedance resonators (UIRs). Then the $\lambda_g/2$ UIRs are grounding at the center and loaded symmetrically with the capacitors C_0 (the capacitance value of C_0 is equal

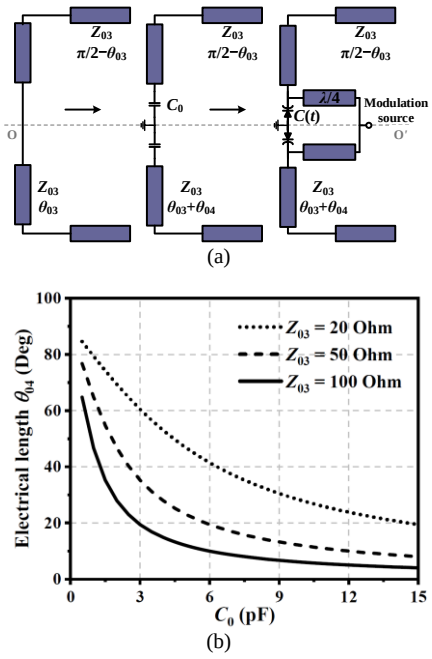

Fig. 3. (a) Evolution of time-modulated resonators and (b) compensated electrical length θ_{04} of the time-modulated resonators against the capacitance C_0.

to that of the reverse biased varactor diodes, which are excited only by DC bias voltage), corresponding to the horizontal plane OO′. It is worth noting that grounding at the center for the $\lambda_g/2$ UIRs does not affect the DM signal owing to the symmetrically loaded RF input and output ports. By adding the electrical length θ_{04} of the UIR, the effect of the loaded capacitance C_0 can be compensated. The relationship between the capacitance C_0 and the transmission line of electrical length θ_{04} is given by the following formula:

$$\omega C_0 + Y_{03} \tan\left(\frac{\pi}{2} + \theta_{04}\right) = 0 \tag{3}$$

where $Y_{03} = 1/Z_{03}$ is the characteristic admittance of the UIR. Figure 3(b) plots the compensated electrical length θ_{04} against the capacitance C_0 for the resonant frequency of $f_0 = 1.5$ GHz. There is a nonlinear relationship between θ_{04} and C_0, which indicates that the resonator's sensitivity to changes in capacitance is dependent on the initial value of C_0. A higher C_0 results in a reduced sensitivity of the resonator to capacitance variations, but a lower C_0 requires a larger θ_{04} leading to an increased resonator size. Thus, the capacitance C_0 from 3 to 9 pF is identified as an appropriate selection for the resonators. Based on the condition, an appropriate varactor diode (Skyworks SMV1234 varactor diode) is selected to achieve the required capacitance C_0 for the resonator. The cathode of the varactor diode is connected to a quarter-wavelength microstrip line, which at the other end is the modulation source (including reverse-biased DC voltage and modulation signal). At the junction of the cathode for the varactor diode and the quarter-wavelength microstrip line, the microstrip line is equivalent to an open circuit at the center frequency f_0. Therefore, the quarter-wavelength microstrip line does not affect the resonance characteristic of the TMR at the center frequency. Moreover, combining with the gap coupling structure of the SIRs, good isolation between RF signal and modulation source is achieved without adding additional lumped elements.

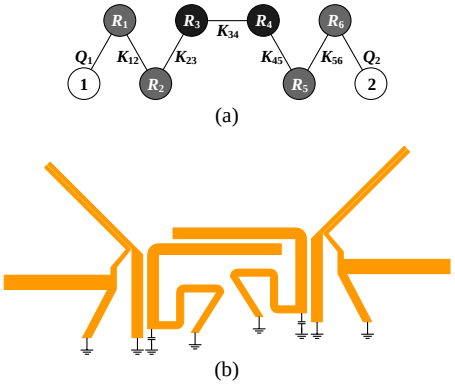

Fig. 4. (a) Coupling topology and (b) odd-mode equivalent circuit of the proposed balanced nonreciprocal BPF.

2.2 Design of Filter without Modulation

The coupling topology of the proposed balanced nonreciprocal BPF is shown in Fig. 4(a), where the white nodes represent the balanced RF input ports and output ports, the gray ones represent the SIRs, the black ones represent the TMRs, $Q_1 = Q_2$ represents the loaded quality factor, and $K_{i,i+1}$ (i = 1, 2, 3, 4, 5) ($K_{12} = K_{56}$, $K_{23} = K_{45}$) represents the coupling coefficient between the resonators R_i and R_{i+1}. The SIRs R_i (i = 1, 2, 5, 6) are used to achieve DM bandpass filtering and CM noise suppression, and the TMRs R_i (i = 3, 4) are used to achieve nonreciprocal characteristics.

The balanced filter exhibits a reciprocal response without modulation. As shown the coupling topology in Fig. 4(a), the proposed filter can realize filtering functionalities by manipulating the coupling coefficients K_{12}, K_{23}, K_{34}, and loaded quality factors Q_1, and the odd-mode equivalent circuit is shown in Fig. 4(b). The loaded quality factors and coupling coefficients can be obtained by

$$Q_1 = \frac{g_0 g_1}{\text{FBW}},\ Q_2 = \frac{g_i g_{i+1}}{\text{FBW}}, \tag{4}$$

$$K_{i,i+1}\big|_{\ i=1 \text{ to } N-1} = \frac{\text{FBW}}{\sqrt{g_i g_{i+1}}} \tag{5}$$

where FBW is the fractional bandwidth, $g_{i,i+1}$ is the element values of the low-pass filter prototype, and N is the order of the filter [19].

The proposed nonreciprocal BPF is designed for a Butterworth response with the center frequency $f_0 = 1.5$ GHz and fractional bandwidth FBW = 16%. Figure 5 shows the simulated results (without modulation) for the tapped coupling position L_q against the loaded quality factor and the coupling gap S_{ci} (i = 1, 2, 3) against the coupling coefficient $K_{i,i+1}$. As expected, after the size of

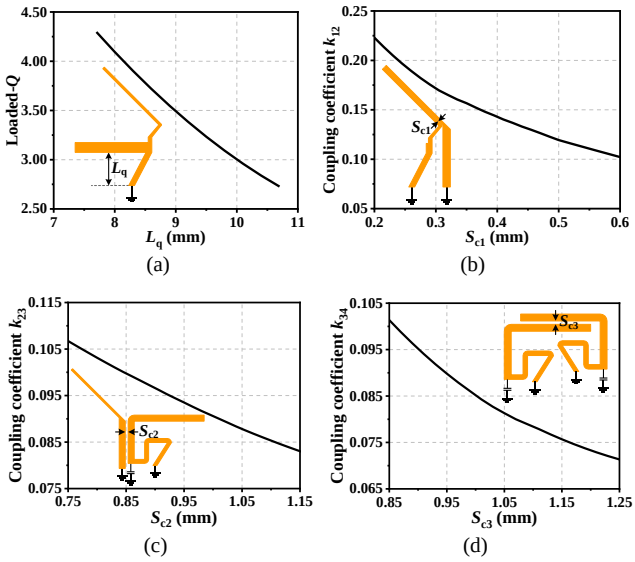

Fig. 5. Related curves about the tapped coupling position and the coupling gap for balanced BPF. (a) Loaded-*Q*. (b) Coupling coefficient K_{12}. (c) Coupling coefficient K_{23}. (d) Coupling coefficient K_{34}.

the resonator is determined, the loaded quality factors and the coupling coefficient of the filters can be adjusted by the tapped coupling position and the coupling gap to satisfy the design specification.

2.3 Modulated Parameterization Analysis

Considering the complexity of the analytical calculation of the balanced nonreciprocal BPF, the parameterization analysis of the modulation parameters (f_m, V_m, and $\Delta\varphi$) is studied as follows. The varactor diode model used in the parametric analysis is the Skyworks SMV1234 varactor, and the colormap is used to effectively depict the parameter sweeping results and represents the variation of modulation parameters.

Forward transmission coefficient ($|S_{ddBA}|$), reverse isolation ($|S_{ddAB}|$), and bandwidth are key indicators for the balanced nonreciprocal bandpass filter. As shown in Figs. 6(a)–6(c), higher f_m values achieve lower forward insertion loss (IL) but result in lower reverse isolation. Higher V_m values achieve higher reverse isolation but result in higher forward IL and smaller 20-dB isolation bandwidth. The modulation parameter $\Delta\varphi$ faced the same questions about trade-off results. Figure 6(d) shows the 20-dB reverse isolation and the 3-dB forward transmission bandwidths against the modulation voltage V_m and the modulation frequency f_m. Lower f_m values achieve wider 3-dB forward transmission bandwidth but result in lower 20-dB reverse isolation bandwidth. The compromise result can be obtained at the intersection of two curves. Based on the foregoing parameterization analysis results, an empirical relationship between the modulation parameters (f_m, V_m, $\Delta\varphi$) and filter specifications (center frequency f_0 and the FBW of the filter when excited only by the DC bias voltage V_{dc}) of the proposed balanced nonreciprocal BPF is built as $f_m = 0.55 \times \text{FBW} \times f_0$, $V_m = 10 \times \text{FBW}$, and

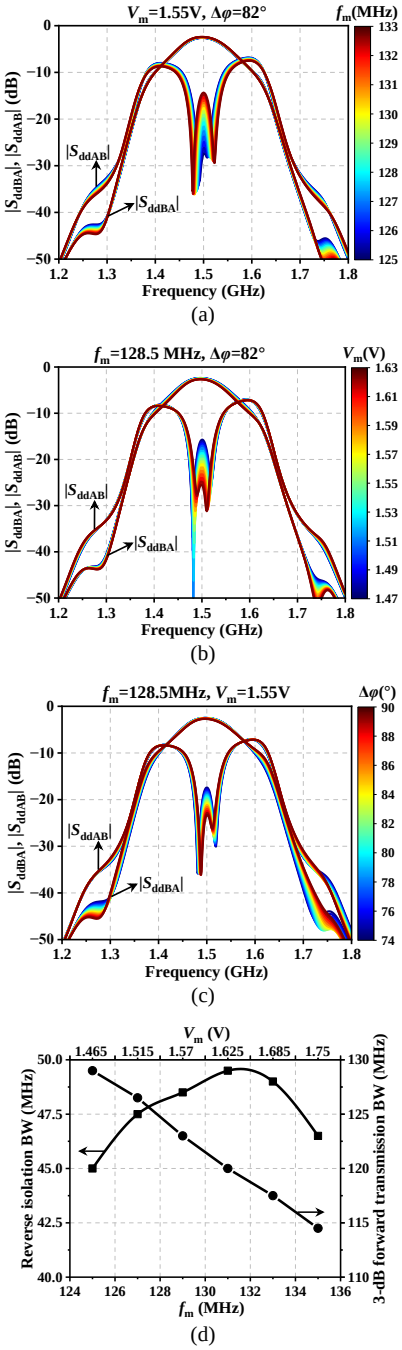

Fig. 6. Simulated forward transmission coefficient and reverse isolation of the proposed balanced nonreciprocal BPF by changing the modulation parameters (a) f_m, (b) V_m, (c) $\Delta\varphi$, and (d) simulated 3-dB forward passband and reverse isolation BWs against f_m and V_m.

$75° < \Delta\varphi < 90°$, which provides a straightforward selection of modulation parameters without need of optimization that can directly be used to reach the BW specifications shown in Fig. 6(d).

Based on the above analysis, the suggested BPF can be developed as follows: At first, based on the analysis results of the resonators, adjust the dimensions of the resonator to make it work at the desired frequency. The second step is to calculate the required loaded quality factor and coupling coefficient according to the specification of the

filter from the element values of the low-pass filter prototype. The third step is to combine the resonators according to the configuration shown in Fig. 3 and tune the tapped coupling position and the coupling gap to get the desired bandpass response (without modulation). The last step is to tune the modulation parameters (f_m, V_m, and $\Delta\varphi$) based on the parameterization analysis to obtain the required nonreciprocal response in the passband.

3. Simulation and Measurement Results

To demonstrate the effectiveness of this design, the proposed balanced nonreciprocal bandpass filter shown in Fig. 7, adopting the design method of the Butterworth response filter, is formulated and measured. The design is performed using co-simulation between ANSYS High-Frequency Structure Simulator (HFSS) and Keysight Advanced Design System (ADS) co-junction with the large signal *S*-parameter analysis module. The filter specifications are the center frequency $f_0 = 1.5$ GHz and FBW = 16% (ranging from 1.38 to 1.62 GHz). An F4B high-frequency substrate with a thickness of 1 mm, a dielectric constant of 2.65, and a loss tangent of 0.003 is used. The required loaded quality factors and coupling coefficients for the novel design in Fig. 7 can be obtained from (4) and (5), which are found to be $Q_1 = Q_2 = 3.376$, $K_{12} = K_{56} = 0.179$, $K_{23} = K_{45} = 0.093$, and $K_{34} = 0.079$. Skyworks SMV1234 varactor diodes are utilized as the time-varying capacitors, and the modulation source are loaded at the varactor diodes via a microstrip line. The overall circuit size of the suggested balanced nonreciprocal BPF is 85 mm × 85 mm, about $0.69\lambda_g \times 0.69\lambda_g$, in which λ_g is the guided wavelength at f_0. The circuit dimensions of the fabricated balanced nonreciprocal BPF microstrip prototypes are given in Tab. 1.

Figure 8 illustrates the simulated and measured reciprocal responses of the BPF, which are only excited by the DC bias voltage $V_{dc} = 1.9$ V. Without modulation, the balanced band-pass filter exhibits a reciprocal response with the measured minimum DM insertion loss of 2.9 dB and the measured maximum DM return loss of 15.6 dB in the DM passband. The measured CM suppression ($|S_{cc21}|$) is better than 57.2 dB in the range of 1.2–1.8 GHz.

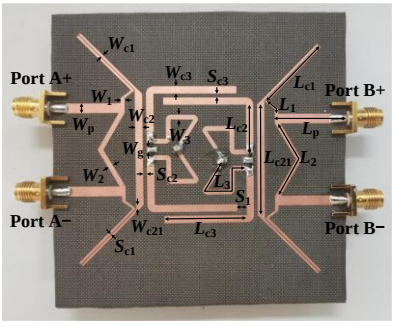

(a)

(b)

Fig. 7. Photograph of the fabricated balanced nonreciprocal BPF: (a) Top. (b) Bottom.

W_{c1}	S_{c1}	L_{c1}	W_{c2}	S_{c2}	L_{c2}	W_{c3}
0.61	0.24	21.90	2.00	0.95	14.30	2.00
S_{c3}	L_{c3}	S_1	W_p	L_p	W_1	L_1
0.95	23.59	2.78	2.72	21.42	1.00	5.25
W_2	L_2	W_{c21}	L_{c21}	W_3	L_3	W_g
1.40	24.20	1.15	32.00	1.33	28.00	1.60

Tab. 1. The circuit dimensions of the proposed balanced nonreciprocal BPF (unit: mm).

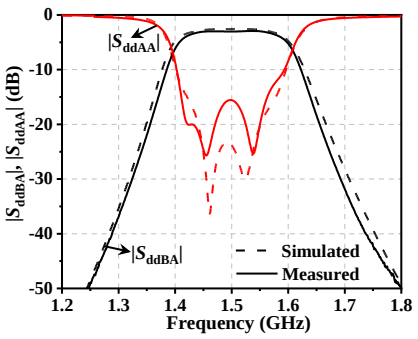

(a)

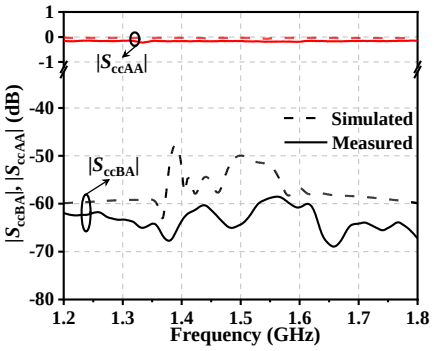

(b)

Fig. 8. Mixed *S*-parameters of the proposed balanced BPF without modulation. (a) DM responses. (b) CM responses.

As shown in Fig. 9, the simulation and measurement results of the proposed balanced nonreciprocal bandpass filter demonstrate good agreement with one another. According to Fig. 9(a), the measured DM minimum in-band forward IL ($|S_{ddBA}|$) is 3.7 dB, and the insertion loss degradation due to modulation (ΔIL) is only 0.8 dB. The meas-

Refs	f_0 (GHz)	Number of TMRs	Poles in reverse isolation	20-dB reverse isolation bandwidth (MHz)	ΔIL (dB)	IL (dB)	RL (dB)	Reverse isolation @f_0 (dB)	Balanced circuit
[12]	0.19	3	2	20	-	1.5	15	20.2	No
[13]	1	3	2	42	1.3	3.9	-	23.2	No
[14]	1.02	2	1	-	2.8	5.5	12	11.7	No
[15]	1.46	2	2	50	1.2	3.1	15.2	20.2	No
[16]	0.96	3	2	-	1.7	4.5	-	18.3	No
[18]	0.725	3	1	-	-	3.2	15	-	Yes
This work	1.5	2	2	48.8	0.8	3.7	24.6	20.5	Yes

Tab. 2. Comparison between this work and other nonreciprocal filters.

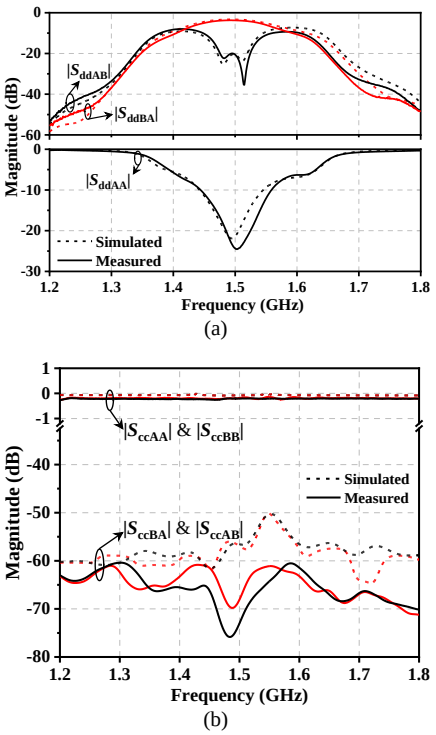

Fig. 9. Simulation and measurement results of the proposed balanced nonreciprocal BPF with modulation. (a) DM responses. (b) CM responses.

ured DM maximum in-band reverse isolation ($|S_{ddAB}|$) is 35 dB, while the bandwidth of reverse isolation better than 20 dB is 48.8 MHz (1.4756 GHz–1.5244 GHz). According to Fig. 9(b), the common-mode suppression is better than 60.4 dB in the range of 1.2–1.8 GHz.

Table 2 presents a comparison between the suggested work and the previous works. The lumped-element filter for achieving nonreciprocal characteristics by using TMRs was first proposed in [12]. The difference of minus one between the number of reverse isolation poles and the number of TMRs in [12]–[14] and [16] means a more complex structure. The balanced nonreciprocal bandpass filter using TMRs was first proposed in [18], but there is only one reverse isolation pole in the 20-dB reverse isolation band. Besides, it adopted the modulation signal feed circuit of lumped elements, which greatly increases its complexity. In contrast, the balanced nonreciprocal BPF proposed in this paper does not use any lumped components except for varactor diodes. Using only two TMRs, two reverse isolation poles have been realized, thus achieving high reverse isolation and wider bandwidth at the same time.

4. Conclusions

In this paper, a novel balanced nonreciprocal bandpass filter based on the stepped impedance resonator and the time-modulated resonator has been presented. Good electromagnetic compatibility characteristics benefit from its balanced structure. Effective isolation between RF and modulation signals is achieved without adding any lumped components. The efficient modulation circuit and the stepped impedance resonator's inherent resonance characteristic build an excellent nonreciprocal characteristic of the differential signal and effective suppression of common-mode noise. Two reverse isolation poles are realized with only two time-modulated resonators. In addition, the proposed design has a simple structure, which is favorable for manufacturing and integration, so it has rich use scenarios in various balanced communication systems.

Acknowledgments

This work was supported by the National Natural Science Foundation of China (No. 61871417), the Liaoning Revitalization Talents Program (No. XLYC2007024), and the Open Fund of Liaoning Key Laboratory of Radio Frequency and Big Data for Intelligent Applications.

References

[1] KORD, A., SOUNAS, D., ALÙ, A. Achieving full-duplex communication: Magnetless parametric circulators for full-duplex

communication systems. *IEEE Microwave Magazine*, 2018, vol. 19, no. 1, p. 84–90. DOI: 10.1109/MMM.2017.2759638

[2] ZHOU, J., REISKARIMIAN, N., DIAKONIKOLAS, J., et al. Integrated full duplex radios. *IEEE Communications Magazine*, 2017, vol. 55, no. 4, p. 142–151. DOI: 10.1109/MCOM.2017.1600583

[3] GHAFFAR, F., BRAY, J., VASEEM, M., et al. Theory and design of tunable full-mode and half-mode ferrite waveguide isolators. *IEEE Transactions on Magnetics*, 2019, vol. 55, no. 8, p. 1–8. DOI: 10.1109/TMAG.2019.2910028

[4] FAY, C., COMSTOCK, R. Operation of the ferrite junction circulator. *IEEE Transactions on Microwave Theory and Techniques*, 1965, vol. 13, no. 1, p. 15–27. DOI: 10.1109/TMTT.1965.1125923

[5] ASHLEY, A., PSYCHOGIOU, D. RF co-designed bandpass filters/isolators using nonreciprocal resonant stages and microwave resonators. *IEEE Transactions on Microwave Theory and Techniques*, 2021, vol. 69, no. 4, p. 2178–2190. DOI: 10.1109/TMTT.2021.3061431

[6] CHANG, J., KAO, J., LIN, Y., et al. Design and analysis of 24-GHz active isolator and quasi-circulator. *IEEE Transactions on Microwave Theory and Techniques*, 2015, vol. 63, no. 8, p. 2638 to 2649. DOI: 10.1109/TMTT.2015.2442976

[7] CARCHON, G., NANWELAERS, B. Power and noise limitations of active circulators. *IEEE Transactions on Microwave Theory and Techniques*, 2000, vol. 48, no. 2, p. 316–319. DOI: 10.1109/22.821785

[8] WEI, F., YU, J., ZHANG, C., et al. Compact balanced dual-band BPFs based on short and open stub loaded resonators with wide common-mode suppression. *IEEE Transactions on Circuits and Systems II: Express Briefs*, 2020, vol. 67, no. 12, p. 3043–3047. DOI: 10.1109/TCSII.2020.2994632

[9] PAN, B., FENG, W., SHI, Y., et al. High-performance wideband balanced bandpass filter based on transversal signal-interference techniques. *IEEE Transactions on Plasma Science*, 2020, vol. 48, no. 12, p. 4119–4126. DOI: 10.1109/TPS.2020.3035558

[10] WEI, F., ZHANG, C., ZENG, C., et al. A reconfigurable balanced dual-band bandpass filter with constant absolute bandwidth and high selectivity. *IEEE Transactions on Microwave Theory and Techniques*, 2021, vol. 69, no. 9, p. 4029–4040. DOI: 10.1109/TMTT.2021.3093907

[11] CHEN, X., YANG, T., CHI, P. Arbitrary-order balanced filter with reflectionless characteristics for both common- and differential-mode signals. *IEEE Microwave and Wireless Components Letters*, 2021, vol. 31, no. 6, p. 553–556. DOI: 10.1109/LMWC.2021.3068469

[12] WU, X., LIU, X., HICKLE, M., et al. Isolating bandpass filters using time-modulated resonators. *IEEE Transactions on Microwave Theory and Techniques*, 2019, vol. 67, no. 6, p. 2331–2345. DOI: 10.1109/TMTT.2019.2908868

[13] WU, X., NAFE, M., MELCÓN, A., et al. Frequency tunable nonreciprocal bandpass filter using time-modulated microstrip $\lambda_g/2$ resonators. *IEEE Transactions on Circuits and Systems II: Express Briefs*, 2021, vol. 68, no. 2, p. 667–671. DOI: 10.1109/TCSII.2020.3014499

[14] WU, X., NAFE, M., MELCÓN, A., et al. A nonreciprocal microstrip bandpass filter based on spatio-temporal modulation. In *IEEE MTT-S International Microwave Symposium*. Boston (MA, USA), 2019, p. 9–12. DOI: 10.1109/MWSYM.2019.8700732

[15] CHAUDHARY, G., JEONG, Y. Nonreciprocal bandpass filter using mixed static and time-modulated resonators. *IEEE Microwave and Wireless Components Letters*, 2022, vol. 32, no. 4, p. 297–300. DOI: 10.1109/LMWC.2021.3123306

[16] ALVAREZ-MELCON, A., WU, X., ZANG, J., et al. Coupling matrix representation of nonreciprocal filters based on time-modulated resonators. *IEEE Transactions on Microwave Theory and Techniques*, 2019, vol. 67, no. 12, p. 4751–4763. DOI: 10.1109/TMTT.2019.2945756

[17] DUTTA, P., KUMAR, G. A., RAM, G. Numerical design of nonreciprocal bandpass filters with the aid of 3D coupling matrix for 5G bands. *IEEE Transactions on Circuits and Systems II: Express Briefs*, 2022, vol. 69, no. 7, p. 3334–3338. DOI: 10.1109/TCSII.2022.3157644

[18] SIMPSON, D., VRYONIDES, P., NIKOLAOU, S., et al. Nonreciprocal balanced bandpass filters with quasi-elliptic response. *IEEE Transactions on Circuits and Systems II: Express Briefs*, 2022, vol. 69, no. 12, p. 5159–5163. DOI: 10.1109/TCSII.2022.3202860

[19] HONG, J. *Microstrip Filters for RF/Microwave Applications*. 2nd ed., rev. Hoboken (NJ, USA): Wiley, 2011. DOI: 10.1002/9780470937297

About the Authors ...

Peng HAN was born in Shijiazhaung, Hebei Province, China. He is currently pursuing his Ph.D. degree in Information and Communication Engineering from DMU. His research interests focus on the balanced microwave circuits and nonreciprocal filters.

Zhongbao WANG (corresponding author) received the Ph.D. degree in Communication and Information Systems from DMU, China, in 2012. He is currently a Full Professor with the School of Information Science and Technology, DMU. From 2014 to 2018, he was a Postdoctoral Fellow with Beijing University of Posts and Telecommunications, China. From 2019 to 2020, he was a Visiting Scholar with the National University of Singapore, Singapore. He has authored more than 90 journal papers. He is currently serving as a Technical Reviewer for the IEEE Transactions on Circuits and Systems, MTT, MWTL, Radioengineering, and so on. His current research interests include balanced RF components and CP antennas.

Hongmei LIU received the Ph.D. degree in Communication and Information Systems from DMU, China, in 2016. She is currently a Full Professor with the School of Information Science and Technology, DMU. Her current research interests include passive microwave circuits, reconfigurable RF components, and CP microwave antennas.

Mingming GAO received the Ph.D. degree in 2015. She is currently an Associate Professor with Liaoning Technical University. Her main research interests include RF circuit and systems, RF device behavior modeling, and artificial intelligence.

Shaojun FANG received the Ph.D. degree in Communication and Information Systems from DMU, China, in 2001. Since 1982, he has been at DMU, where he is currently the Head Professor with the School of Information Science and Technology. His recent research interests include passive RF components and antennas.